J. Fluid Mech. (1979), *vol.* 94, *part* 4, *pp.* 777–793
Printed in Great Britain

Numerical calculations of steady gravity–capillary waves using an integro-differential formulation

By JAMES W. ROTTMAN AND D. B. OLFE

Department of Applied Mechanics and Engineering Sciences, University of California, San Diego, La Jolla, California 92093

(Received 8 August 1978 and in revised form 7 February 1979)

A new integro-differential equation is derived for steady free-surface waves. Numerical solutions of this equation for periodic gravity–capillary waves on a fluid of infinite depth are presented. For the two limiting cases of gravity waves and capillary waves, our results are in excellent agreement with previous calculations. For gravity–capillary waves, detailed calculations are performed near the wavenumber at which the classical second-order perturbation solution breaks down. Our calculations yield two solutions in this region, which in the limit of small amplitudes agree with the results obtained by Wilton in 1915; one solution has the small amplitude behaviour of a gravity wave and the other that of a capillary wave, but the numerical results show that at large amplitudes both waves have the characteristics of capillary waves. The calculations also show that the wavenumber range in which two solutions exist increases with increasing wave height.

1. Introduction

The study of steady irrotational water waves is a classical branch of fluid mechanics that has received a considerable amount of attention. The early investigations of the nonlinear behaviour of periodic irrotational water waves on deep water consisted of perturbation solutions that are valid when the maximum wave slope is small. Stokes (1847, 1880*a*) pioneered the field by developing perturbation expansion procedures for the approximate calculation of gravity waves propagating on a free surface. These procedures have been extended by Harrison (1909), Wilton (1915), and Pierson & Fife (1961) to include the effects of surface tension.

For gravity waves Stokes' solution shows that nonlinear waves have sharper crests and broader troughs compared to sinusoidal waves and that the phase speed of nonlinear waves increases with increasing wave height. For gravity–capillary waves Harrison's solution shows that the basic characteristics of Stokes' waves are retained for wavenumbers less than $k_2 = (\rho g/2\sigma)^{\frac{1}{2}}$, where ρ is the density, g is the acceleration of gravity, and σ is the surface tension. However, for wavenumbers greater than this dividing wavenumber, the waves have the general characteristics of capillary waves; the wave profiles have flattened crests and sharp troughs and phase speeds which decrease with increasing wave height. Harrison noted, however, that his solution breaks down at the dividing wavenumber. Wilton independently computed a solution to Harrison's problem to higher order. Additional singularities appear in the higher-order terms at the wavenumbers $k_n = (\rho g/n\sigma)^{\frac{1}{2}}$, where n is an integer greater than unity. Wilton also developed another perturbation solution that is valid exactly at

0022-1120/79/4319-7600 $02.00

Harrison's dividing wavenumber, which shows that two distinct waves exist with this wavenumber. Pierson & Fife used the method of strained co-ordinates to determine a perturbation solution that is valid for a small band of wavenumbers centred about Harrison's dividing wavenumber. Their results show that two distinct waves exist at wavenumbers near the dividing wavenumber.

In recent years, the computer has been used to obtain more accurate information on the nonlinear behaviour of water waves when the maximum wave slope is not small. Thomas (1968, 1975) used the computer to solve an integral equation for gravity waves derived by Nekrasov (1921). Byatt-Smith (1970) derived another integral equation for gravity waves, and he numerically solved this equation for the case of the solitary wave. Sasaki & Murakami (1973) numerically solved yet another integral equation for gravity waves on fluids of various depths, including the solitary wave. Schwartz (1974), Longuet-Higgins (1975), and Cokelet (1977) used the computer to extend the Stokes series for gravity waves to very high order. The numerical calculations have shown the crests of gravity waves increase in sharpness as the height increases until a limiting waveform is reached in which the crest is a corner enclosing an angle of 120°, as Stokes (1880*b*) conjectured. Another interesting result, originally due to Longuet-Higgins, is that the wave properties, such as the phase speed and the wave energy, are found to monotonically increase to maxima just before the wave reaches maximum height. Very recently, Bloor (1978) derived an integro-differential equation for surface waves which includes the effects of surface tension as well as gravity. Although it appears that his equation could be used to calculate gravity–capillary waves, he presented numerical results only for the two limiting cases of pure gravity waves and pure capillary waves.

In the present work we introduce a new integro-differential equation that describes free-surface gravity–capillary waves. This equation differs substantially from that of Bloor, and offers advantages for the computation of periodic waves. We present numerical results for deep-water gravity waves, capillary waves, and gravity–capillary waves with wavenumbers near Harrison's dividing wavenumber.

2. Formulation of the problem

Consider two-dimensional, periodic, progressive waves of wavelength λ propagating on the free surface of a fluid of arbitrary uniform depth h. Assume that the fluid is inviscid, incompressible, and that the motion is irrotational.

Define a Cartesian co-ordinate system in a reference frame in which the motion is steady, such that the x axis is horizontal and the y axis is perpendicular to the undisturbed surface and directed opposite to the force of gravity. Take the bottom to lie along $y = 0$ and define a mean depth h such that the surface is given by $y = h + \eta(x)$, with the value of η averaged over one wavelength set equal to zero. In this reference frame, define the value of the fluid speed averaged over one wavelength at $y = 0$ to be the phase speed c of the wave; since the motion is irrotational, the result would be the same for any value of y. One wavelength of the flow is illustrated in figure 1.

Let u and v represent the components of fluid velocity in the x and y directions, respectively, and define the complex velocity of the flow as

$$w(z) = u - iv, \tag{1}$$

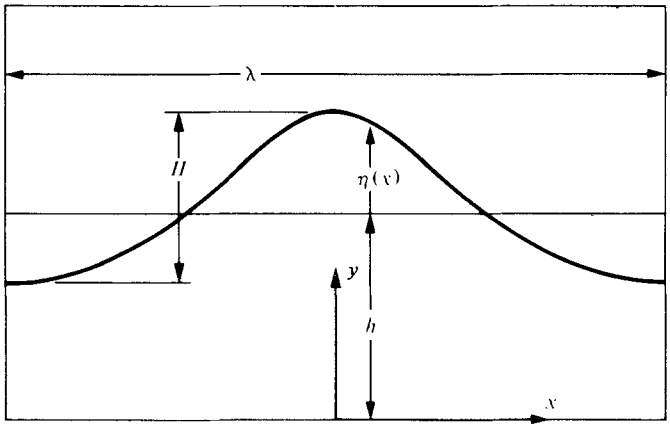

FIGURE 1. A schematic representation of the surface profile over one wavelength.

where $z = x+iy$. The problem is to determine the function $w(z)$ that is analytic in the fluid region, the phase speed c, and the shape of the free surface $\eta(x)$ such that the following boundary conditions are satisfied:

$$v = 0 \qquad \text{on} \quad y = 0, \tag{2}$$

$$v - u\eta_x = 0 \qquad \text{on} \quad y = h+\eta(x), \tag{3}$$

$$p - p_0 = -\sigma R^{-1} \quad \text{on} \quad y = h+\eta(x), \tag{4}$$

where p is the fluid pressure, p_0 is the constant pressure above the surface, σ is the surface tension, and R is the radius of curvature of the free surface. The pressure in the fluid at the surface is related to the fluid speed by the Bernoulli equation

$$p/\rho + \tfrac{1}{2}(u^2+v^2) + g\eta = B, \tag{5}$$

in which B is a constant.

To obtain an integro-differential formulation of this problem, we seek to express the complex velocity in terms of its values on the surface. Since the complex velocity is analytic in the fluid region, we can use Cauchy's integral theorem to express the complex velocity in the interior as an integral over its values on the boundary of the fluid region,

$$w(z) = \frac{1}{2\pi i}\oint \frac{w(\zeta)}{\zeta - z}\,d\zeta. \tag{6}$$

In the limit as the integration path extends to infinity in the horizontal direction, the contributions from the two paths connecting the bottom to the surface independently vanish, so the non-zero contributions to this integral come from the paths along the free surface and the fluid bottom. The integration along the bottom can be eliminated by adding an image flow, which satisfies (2). Boundary condition (3) implies that on the free surface

$$w(\zeta)\,d\zeta = q\,ds, \tag{7}$$

where q is the fluid speed at the free surface and ds is the differential arc length along the free surface. Thus, including the image flow, (6) may be written as

$$w(z) = \frac{1}{2\pi i}\int_{-\infty}^{\infty}\left(\frac{1}{\zeta^* - z} - \frac{1}{\zeta - z}\right)\gamma(\xi)\,d\xi, \tag{8}$$

where $\zeta = \xi + i(h+\eta)$, ζ^* is the complex conjugate of ζ, and

$$\gamma(\xi) \equiv q(1+\eta_\xi^2)^{\frac{1}{2}}. \tag{9}$$

From (4) and (5)

$$q = \left(2B + 2\frac{\sigma}{\rho}R^{-1} - 2g\eta\right)^{\frac{1}{2}}, \tag{10}$$

so (8), therefore, expresses the complex velocity in the interior of the fluid region in terms of η and the constants of the motion. For the particular case of periodic waves, (8) can be expressed as

$$\begin{aligned} w(z) &= \frac{1}{2\pi i}\sum_{n=-\infty}^{\infty}\int_{\frac{1}{2}(2n-1)\lambda}^{\frac{1}{2}(2n+1)\lambda}\left(\frac{1}{\zeta^*-z}-\frac{1}{\zeta-z}\right)\gamma(\xi)\,d\xi \\ &= \frac{1}{2\pi i}\int_{-\frac{1}{2}\lambda}^{\frac{1}{2}\lambda}\gamma(\xi)\sum_{n=-\infty}^{\infty}\left\{\frac{1}{[\xi+n\lambda-i(h+\eta)]-z}-\frac{1}{[\xi+n\lambda+i(h+\eta)]-z}\right\}d\xi \\ &= \frac{1}{2\lambda i}\int_{-\frac{1}{2}\lambda}^{\frac{1}{2}\lambda}\{\cot[\pi(\zeta^*-z)/\lambda]-\cot[\pi(\zeta-z)/\lambda]\}\gamma(\xi)\,d\xi. \end{aligned} \tag{11}$$

The last step follows from Mittag-Leffler's expansion of the cotangent function (Whittaker & Watson 1927).

On the surface, $z_s = x+i(h+\eta)$, and the integrals in (8) and (11) are singular. However, the Plemelj formulae (see, e.g., Muskhelishvili, 1953) can be employed to show that $w(z_s)$ is equal to twice the Cauchy principal value of these singular integrals. Interpreting (8) accordingly, separating its real and imaginary parts, and substituting these into (3), we obtain the following equation for η:

$$-\frac{1}{\pi}P\int_{-\infty}^{\infty}\left\{\frac{(x-\xi)+[\eta(x)+\eta(\xi)+2h]\,\eta_x}{(x-\xi)^2+[\eta(x)+\eta(\xi)+2h]^2}-\frac{(x-\xi)+[\eta(x)-\eta(\xi)]\,\eta_x}{(x-\xi)^2+[\eta(x)-\eta(\xi)]^2}\right\}\gamma(\xi)\,d\xi = 0, \tag{12}$$

where P stands for Cauchy principal value. Integrating this expression with respect to x results in the following integro-differential equation for η:

$$\frac{1}{2\pi}P\int_{-\infty}^{\infty}\ln\left\{\frac{(x-\xi)^2+[\eta(x)-\eta(\xi)]^2}{(x-\xi)^2+[\eta(x)+\eta(\xi)+2h]^2}\right\}\gamma(\xi)\,d\xi = \text{constant}. \tag{13}$$

For periodic flows, the same procedure using (11) instead of (8) produces

$$\frac{1}{2\pi}P\int_{-\frac{1}{2}\lambda}^{\frac{1}{2}\lambda}\ln\left\{\frac{\cosh\{k[\eta(x)-\eta(\xi)]\}-\cos\{k(x-\xi)\}}{\cosh\{k[\eta(x)+\eta(\xi)+2h]-\cos\{k(x-\xi)\}}\right\}\gamma(\xi)\,d\xi + K = 0, \tag{14}$$

where $k = 2\pi/\lambda$ and K is the integration constant.

As a check on the validity of this formulation, approximate periodic solutions valid for small wave slopes were obtained for equation (13). The results were found to be in agreement with the existing small amplitude solutions. The details are given in Rottman (1978).

Equation (14) represents an integro-differential equation by which the surface profile η is determined directly in terms of x, with the fluid depth h and the wavelength λ appearing explicitly as parameters in the equation. In contrast, the integro-differential equation of Bloor (1978) is solved for $\alpha(r)$, where α is the local angle of the surface and r is a transformed position variable. In order to evaluate the surface profile $\eta(x)$ and determine the values of h and λ, additional integrals involving $\alpha(r)$ must be evaluated. Furthermore, the integral appearing in Bloor's basic integro-

differential equation extends over an infinite interval, compared to the finite interval of (14). One advantage of Bloor's equation is that unlike (14) it can be used to calculate very large amplitude capillary wave profiles for which $\eta(x)$ becomes multi-valued.

3. Numerical method

The algorithm

We consider here the numerical solution of the integro-differential equation for periodic free-surface waves on a fluid of infinite depth. For this purpose, all quantities are made non-dimensional by referencing all lengths to $1/k$ and all velocities to $(g/k)^{\frac{1}{2}}$. The resulting non-dimensional parameter is $\tilde{\sigma} \equiv \sigma k^2/\rho g$. Thus, taking the limit of (14) as h tends to infinity gives

$$c\eta(x) = \frac{1}{2\pi} P \int_{-\pi}^{\pi} \gamma(\xi) \ln \{\cosh [\eta(x) - \eta(\xi)] - \cos (x - \xi)\} \, d\xi + K_\infty, \tag{15}$$

where
$$\gamma(\xi) = (c^2 + 2\tilde{\sigma} R^{-1} - 2\eta)^{\frac{1}{2}} (1 + \eta_\xi^2)^{\frac{1}{2}}, \tag{16}$$
and K_∞ is a constant.

Since η and γ are periodic functions of period 2π, (15) can be written in the form

$$c\eta(x) = \frac{1}{2\pi} \int_0^{\pi} [\gamma(x-\tau) \ln \{\cosh [\eta(x) - \eta(x-\tau)] - \cos \tau\} + \gamma(x+\tau) \ln \{\cosh [\eta(x) - \eta(x+\tau)] - \cos \tau\}] \, d\tau + K_\infty, \tag{17}$$

which conveniently places the singularity in the integrand at the lower limit of integration. The integrand has a logarithmic singularity at $\tau = 0$. This is made clearer by expanding the integrand for small τ; the result is

$$2\gamma(x) \ln [\tfrac{1}{2}(1 + \eta_x^2) \tau^2] + O(\tau^2 \ln \tau). \tag{18}$$

The singularity can be subtracted out of the integrand using the result

$$\frac{1}{2\pi} \int_0^{\pi} 2\gamma(x) \ln [\tfrac{1}{2}(1 + \eta_x^2) \tau^2] \, d\tau = \gamma(x) \{\ln [\tfrac{1}{2}(1 + \eta_x^2) \pi^2] - 2\},$$

so that equation (17) can be written as

$$\begin{aligned} c\eta(x) = \frac{1}{2\pi} \int_0^{\pi} & [\gamma(x-\tau) \ln \{\cosh [\eta(x) - \eta(x-\tau)] - \cos \tau\} \\ & + \gamma(x+\tau) \ln \{\cosh [\eta(x) - \eta(x+\tau)] - \cos \tau\} - 2\gamma(x) [\ln \tfrac{1}{2}(1 + \eta_\tau^2) \tau^2]] \, d\tau \\ & + \gamma(x) \{\ln [\tfrac{1}{2}(1 + \eta_x^2) \pi^2] - 2\} + K_\infty. \end{aligned} \tag{19}$$

Although the integrand is now finite on $(0, \pi)$, not all of its derivatives are finite at $\tau = 0$; this fact has important implications for the error analysis to be carried out later.

To obtain a numerical solution of (19) we determine η at N equally spaced points on the interval $(0, \pi)$. Denoting these points by

$$x_i = (i-1) \Delta x; \quad \tau_j = (j-1) \Delta \tau; \quad i, j = 1, 2, \ldots, N,$$

where $\Delta x = \Delta \tau = \pi/(N-1)$, and, letting $\eta_i = \eta(x_i)$ and $\gamma_i = \gamma(x_i)$, we approximate the integral in (19) by Simpson's rule and the derivatives by fourth-order difference

formulae. Then $N+2$ nonlinear algebraic equations for the $N+2$ unknowns η_i, c, and K_∞ result from (19) together with the requirement that the mean value of η be zero and the requirement that the wave height (or some parameter related to the wave height) have a fixed value.

There are many numerical techniques for solving this type of problem, and it seems that experimentation is the only means for determining which method is best for a particular system. We found that the Newton–Raphson iteration method for a system of equations worked well. Schematically, the numerical procedure is as follows.

Let the $N+2$ equations to be solved be represented by

$$F_i(\eta_j) = 0; \quad i,j = 1, 2, \ldots, N, N+1, N+2, \tag{20}$$

where for notational convenience we have defined $\eta_{N+1} \equiv c$ and $\eta_{N+2} \equiv K_\infty$. The first step is to approximate the η_j's; this is done by using a perturbation solution or by using a previously computed profile which is near the desired solution. Denote this first approximation by a superscript zero, $\eta_j^{(0)}$, and denote the residual by E_i; that is

$$F_i(\eta_j^{(0)}) = E_i. \tag{21}$$

Assuming that the E_i are small, corrections to the $\eta_j^{(0)}$ are found by expanding F_i in a Taylor series about $\eta_j^{(0)}$:

$$F_i(\eta_j^{(0)} - \Delta\eta_j) \simeq E_i - \left.\frac{\partial F_i}{\partial \eta_j}\right|_{\eta_j = \eta_j^{(0)}} \Delta\eta_j. \tag{22}$$

After setting F_i equal to zero, the resulting linear system of equations (22) is solved for the corrections $\Delta\eta_j$. Thus the new approximation is $\eta_j^{(1)} = \eta_j^{(0)} - \Delta\eta_j$. This procedure is then repeated until the E_i's are reduced in absolute value to some prescribed tolerance. For the calculations done here, this tolerance is 10^{-8}.

In all of the calculations presented here, the assumption is made that the waves are symmetric about a vertical plane passing through their crests, so that only one half-wavelength of the wave profile is actually computed. Levi-Civita (1925) proved the existence of steady irrotational gravity waves that have this property, and the exact result of Crapper (1957) shows that capillary waves are also symmetric.

After the solution is obtained, the integral properties, such as the mean kinetic energy per unit area T, the mean gravitational potential energy per unit area V, and the surface energy per unit area S, are computed using Simpson's rule. These quantities are given by

$$T = -\frac{c}{4\pi}\int_{-\pi}^{\pi} \gamma\eta\, dx, \quad V = \frac{1}{4\pi}\int_{-\pi}^{\pi} \eta^2\, dx, \tag{23), (24}$$

and

$$S = \frac{\tilde{\sigma}}{2\pi}\int_{-\pi}^{\pi} (1+\eta_x^2)^{\frac{1}{2}}\, dx - \tilde{\sigma}. \tag{25}$$

Error analysis and extrapolation

Fox (1967) derived an expression for Simpson's rule, with correction terms appropriate for an integrand with discontinuous derivatives at the lower limit of integration. Contrary to the expression for smooth integrands, the dependence of Fox's correction

terms on the interval length, $\Delta\tau$, is a function of the integrand. For the integrand in (19), the correction formula has the form

$$A(\Delta\tau)^3 + B(\Delta\tau)^4 + C(\Delta\tau)^5 \ln(\Delta\tau) + D(\Delta\tau)^5 + \ldots, \tag{26}$$

where the coefficients A, B, etc. are independent of $\Delta\tau$. For our finite-difference approximation to the derivatives we can expect the largest error to be of order $(\Delta\tau)^4$. Therefore, we estimate that the error in our calculations is approximately given by

$$e \simeq A(\Delta\tau)^3 + B(\Delta\tau)^4. \tag{27}$$

The approximate error can be computed by solving equation (19) for three different step sizes ($\Delta\tau$) and using these results to determine A, B, and the extrapolated solution. This procedure is simply Richardson's extrapolation, and it was used to achieve the accurate numerical results presented in the next section.

Some identical calculations were made on a CDC 3600 computer and on a CDC 7600 computer with identical results. Since the latter computer has approximately 36% greater single precision accuracy than the former, this indicates that the round-off error in these calculations is insignificant.

4. Numerical results

Gravity waves

We are now in a position to compute the solution for periodic gravity waves. Our results will be compared with those of Cokelet (1977), whose summation of large-order perturbation series was facilitated by the use of Padé approximants, a technique introduced into water wave theory by Schwartz (1974). Our calculations serve both to verify the accuracy of the present computational technique and to confirm the validity of the use of Padé-approximant techniques in water wave problems.

For these calculations we use the following convenient parameter introduced by Cokelet:

$$\epsilon^2 = 1 - \frac{q_{\text{crest}}^2 q_{\text{trough}}^2}{c^4}.$$

This parameter approaches zero as the gravity wave amplitude approaches zero, and monotonically increases to unity as the wave increases to maximum amplitude.

To estimate the error and to carry out Richardson's extrapolation as discussed in the preceding section, each wave profile was computed for three different step sizes, $\Delta\tau$. It was found, for wave heights for which $\epsilon^2 < 0{\cdot}95$, that sufficient accuracy is obtained by dividing the half-wavelength into 48, 72, and 96 equal intervals for the three computations. For wave amplitudes for which $\epsilon^2 \geqslant 0{\cdot}95$, the number of intervals was increased to 60, 90, and 120 for the three calculations. This ensured that the wave speed was computed to five-place accuracy up to $\epsilon^2 = 0{\cdot}98$. The accuracy of the calculation degraded quite rapidly for $\epsilon^2 > 0{\cdot}98$, as the curvature near the crest becomes very large.

The numerical procedure converged very rapidly, taking at the most four iterations, for all wave amplitudes up to $\epsilon^2 = 0{\cdot}999$. The average execution time for computing one profile was approximately 90 seconds on a CDC 3600 computer and 6 seconds on a CDC 7600 computer.

ϵ^2	c	c (Cokelet)
0·900	1·09094	1·09094
0·920	1·09202	1·09202
0·940	1·09272	1·09272
0·950	1·09290	1·09290
0·960	1·09295	1·09295
0·970	1·09288	1·09287
0·980	1·09268	1·09266
0·990	1·0924	1·09238
0·999	1·0919	—
1·000	—	1·0922

TABLE 1. The phase speed c of gravity waves as a function of the parameter ϵ^2. The second column contains the c values obtained from the present calculation, whereas the third column contains the values calculated by Cokelet (1977).

As an example of Richardson's extrapolation procedure we consider the wave speed for $\epsilon^2 = 0{\cdot}98$. The three values of the phase speed calculated for $\Delta\tau_1 = \pi/60$, $\Delta\tau_2 = \pi/90$, and $\Delta\tau_3 = \pi/120$ are used to give the following three equations involving A, B, and c:

$$c = 1{\cdot}092534 + A(\Delta\tau_1)^3 + B(\Delta\tau_1)^4,$$
$$c = 1{\cdot}092585 + A(\Delta\tau_2)^3 + B(\Delta\tau_2)^4,$$
$$c = 1{\cdot}092629 + A(\Delta\tau_3)^3 + B(\Delta\tau_3)^4.$$

Solving these equations we find $A = 4{\cdot}521$, $B = -67{\cdot}110$, and an extrapolated wave speed $c = 1{\cdot}09268$. This extrapolated c differs by $e = 0{\cdot}00005$ from the c value calculated using $\Delta\tau_3$, and by only 0·00002 from the value $c = 1{\cdot}09266$ calculated by Cokelet (1977).

The extrapolated values of the phase speed obtained for values of ϵ^2 in the range $0{\cdot}90 \leqslant \epsilon^2 < 1{\cdot}00$ are given in the second column of table 1. The third column contains the values obtained by Cokelet (1977) using Padé approximants. The largest differences between the two calculations are at the wave heights very near the maximum wave height where, as has already been pointed out, the present calculation shows substantial numerical error. In any case, the maximum difference in the two calculations is only about 0·03 % of the total variation of c.

Similar agreement was obtained for the wave profiles, and for the calculated values of the kinetic and potential energies; see Rottman (1978).

Capillary waves

The numerical scheme of § 3 was applied to the case of a capillary wave, with the linear capillary phase speed used for nondimensionalization purposes. Execution times and convergence rates were similar to those for the gravity wave case. The numerical procedure, using a maximum of 120 intervals, could easily compute wave profiles for all amplitudes up to $H/\lambda = 0{\cdot}5$. Beyond this wave height the numerical procedure showed difficulty in approximating the steep slopes. In fact, at amplitudes somewhat greater than $H/\lambda = 0{\cdot}5$, an infinite slope appears in the wave profile and $\eta(x)$ becomes multi-valued, which is a situation that cannot be handled by our computational procedure. The theoretical maximum height is $H/\lambda = 0{\cdot}73$, which corres-

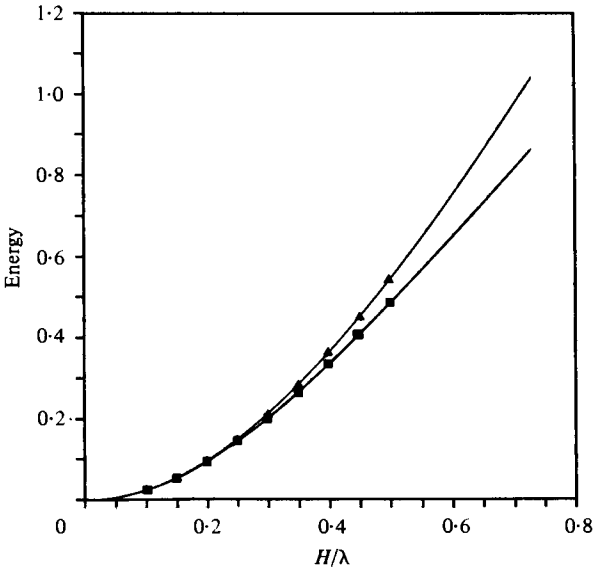

FIGURE 2. The calculated values of the kinetic energy (■) and the surface energy (▲) of capillary waves as functions of the wave height, compared with the exact results (solid lines) of Crapper (1957).

ponds to a bubble of air being pinched off in the narrow trough of the capillary wave (see Crapper, 1957).

The computed phase speed showed excellent agreement with Crapper's solution, with seven-place accuracy being achieved for $H/\lambda < 0{\cdot}4$. In contrast to the gravity wave case, the capillary phase speed decreases with increasing amplitude for all amplitudes. Rather than presenting the phase speed results (for which Crapper has given a simple exact formula), we choose to present our results for the kinetic and surface energies because, as far as we know, these calculations have not been previously presented. Figure 2 shows our computed kinetic and surface energies, compared with values (solid lines) calculated directly from Crapper's solution by the numerical evaluation of integrals (23) and (25). In addition to illustrating the accuracy of our numerical method, the figure shows that the surface energy exceeds the kinetic energy at finite amplitudes. This is in contrast to the gravity wave case, where for finite amplitudes the kinetic energy exceeds the gravitational potential energy.

Gravity–capillary waves

The preceding subsections have shown that nonlinearity has nearly opposite effects in the two limiting cases of gravity waves ($\tilde{\sigma} \to 0$) and capillary waves ($\tilde{\sigma} \to \infty$). Therefore, it is interesting to see how these effects are exhibited in a wave where the effects of gravity and surface tension are of approximately equal importance. In the linear theory of gravity–capillary waves, the phase speed has a minimum at the wavenumber for which $\tilde{\sigma} = 1$, and Kelvin (1910) suggested that this wavenumber should be considered the dividing line between capillary-like waves (waves in which surface tension effects dominate over gravity effects) and gravity-like waves. However, the existing higher-order theories for gravity–capillary waves indicate that the wave

corresponding to $\tilde{\sigma} = 1$ is really more of a capillary-like wave. Our calculations (Rottman 1978) confirm the fact that the $\tilde{\sigma} = 1$ wave is capillary-like; namely, the wave profile has narrow troughs and broad crests, the phase speed is a monotonically decreasing function of wave height, and the surface energy exceeds the gravitational potential energy at finite amplitudes (also, the sum of the surface and gravitational potential energies exceeds the kinetic energy).

Gravity and surface tension effects are of approximately equal importance at the singular point $\tilde{\sigma} = \frac{1}{2}$. The perturbation analysis of Wilton (1915) predicts two distinct solutions at $\tilde{\sigma} = \frac{1}{2}$, one solution being a gravity-like wave and the other solution being capillary-like. In the remainder of this section our numerical scheme will be used to examine the nature of the gravity–capillary wave solutions in the vicinity of $\tilde{\sigma} = \frac{1}{2}$.

The method of extrapolation and error analysis is the same as that used in the previous section on gravity waves. The convergence rates and execution times were also found to be similar to the gravity case. In all of these calculations, 120 was the largest number of intervals used.

For our calculations near $\tilde{\sigma} = \frac{1}{2}$ we consider the gravity-like wave first. The procedure adopted for computing these waves was to initially compute the waves for which $\tilde{\sigma} = 0{\cdot}42$, which is approximately half-way between the first two singular points located at $\tilde{\sigma} = \frac{1}{2}$ and $\frac{1}{3}$, using the approximate solution of Harrison (1909) to start the calculations. Next, the value of $\tilde{\sigma}$ was increased and the previously computed results were used as initial approximations for calculating the waves at this new value of $\tilde{\sigma}$. This procedure was then repeated until a value of $\tilde{\sigma}$ was reached at which, as it turns out, the wave became indistinguishable from a wave half the wavelength; that is, the wave disappears at a small distance (which increases with wave height) to the large wavenumber side of the singular point. This disappearance occurs when the amplitudes of the fundamental and all odd multiples of the fundamental become zero, leaving a wave which is identical to a capillary-like wave of twice the (disappearing) fundamental wavenumber. This process is described in more detail below.

Figure 3 shows the wave profiles computed at $\tilde{\sigma} = 0{\cdot}50$. The smallest-amplitude profile has the gravity-wave characteristic of narrower crest than trough, but, as the wave height increases, a local maximum appears in the trough. Thus, the profile exhibits two local minima per wavelength. The trough tends to sharpen as the wave height increases. In contrast, the crest tends to flatten with increasing wave height so that the larger amplitude waves look like capillary waves with a bump in their troughs. Similar statements can be made about waves that were computed at $\tilde{\sigma} = 0{\cdot}42$ and $0{\cdot}58$. Also, we note that the maximum wave height we can compute increases as $\tilde{\sigma}$ increases.

Figure 4 is a plot of the phase speed versus wave height for the three values $\tilde{\sigma} = 0{\cdot}42$, $0{\cdot}50$, and $0{\cdot}58$. Also included in the plot are the phase speeds computed from the second-order perturbation solution of Pierson & Fife (1961). The numerical results show the phase speed increasing for small wave heights but then reaching a maximum and declining for larger wave heights. The perturbation results predict that the phase speed only increases with wave height. The maximum in the phase speed seems to occur at slightly larger wave heights for larger values of $\tilde{\sigma}$ but in all cases it is close to $H/\lambda = 0{\cdot}05$, which indicates that the perturbation solution is valid for very small amplitudes only. It also appears that the perturbation solution, even for small amplitudes, is only accurate near $\tilde{\sigma} = 0{\cdot}50$. The decreasing of the phase speed with large

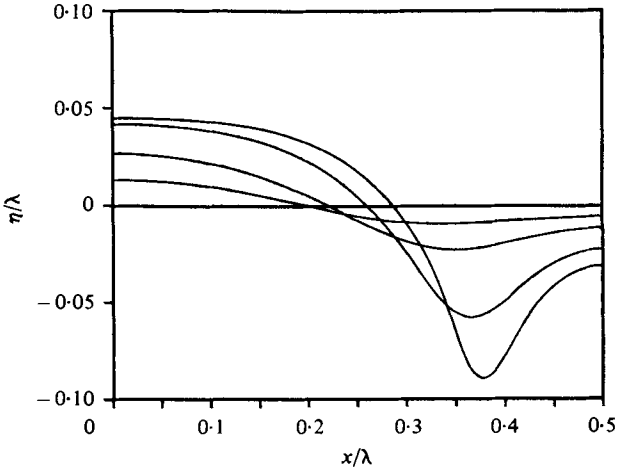

FIGURE 3. Surface profiles of the wave that is gravity-like for small amplitudes, with $\tilde{\sigma} = 0{\cdot}50$, and $H/\lambda = 0{\cdot}02$, $0{\cdot}05$, $0{\cdot}10$, and $0{\cdot}13$. One half-wavelength is shown.

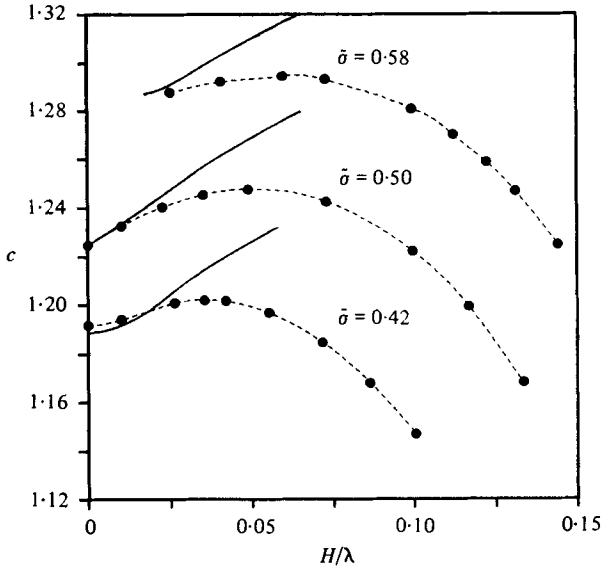

FIGURE 4. The phase speed as a function of the wave height for waves that are gravity-like at small amplitudes. The present results (●) are compared with the approximate solutions (solid lines) of Pierson & Fife (1961). The dashed lines are spline fits to the present results.

wave heights is in agreement with the earlier observation that these waves are gravity-like for small wave heights, and more capillary-like for larger wave heights.

The wave energies versus the wave height for $\tilde{\sigma} = 0{\cdot}50$ are plotted in figure 5. The results computed for $\tilde{\sigma} = 0{\cdot}42$ and $0{\cdot}58$ are very similar to these results. This plot indicates, again, that these waves have the large amplitude behaviour of capillary waves; the surface energy exceeds the gravitational potential energy (and the sum of the surface and gravitational potential energies exceeds the kinetic energy for large wave heights).

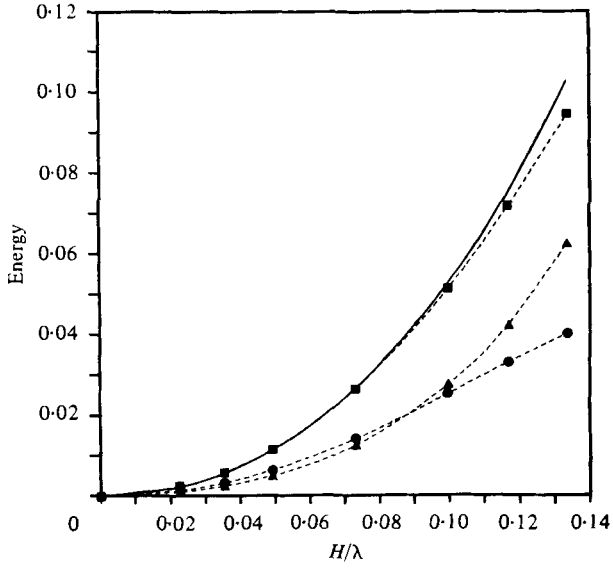

FIGURE 5. The calculated values of the kinetic energy (■), surface energy (▲) and gravitational potential energy (●) as functions of the wave height, calculated at $\tilde{\sigma} = 0{\cdot}50$ for a wave which is gravity-like at small amplitudes. The dashed lines are spline fits to the present results, and the solid line is the sum of the surface and gravitational potential energies.

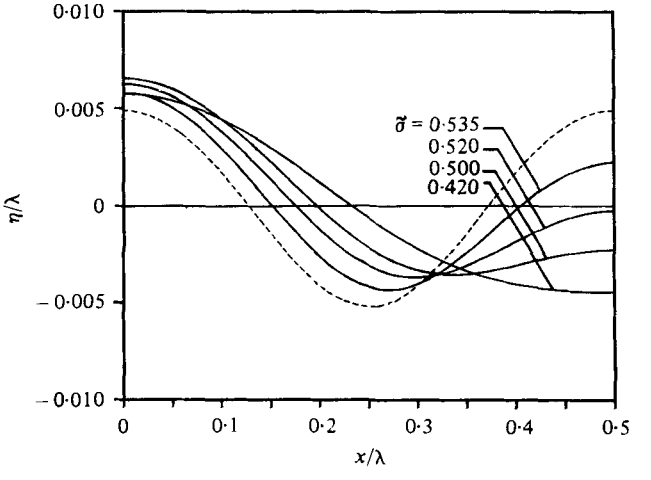

FIGURE 6. Surface profiles for the wave which is gravity-like at small amplitudes, calculated for $H/\lambda = 0{\cdot}01$ and various values of $\tilde{\sigma}$. The dashed line represents the profile for both $\tilde{\sigma} = 0{\cdot}545$ and $\tilde{\sigma} = 2{\cdot}18$.

The behaviour of these waves with $\tilde{\sigma}$, for two fixed wave height to wavelength ratios, $H/\lambda = 0{\cdot}01$ and $0{\cdot}10$, is shown in figures 6 and 7. There are two results to be noted from these plots. First, as $\tilde{\sigma}$ increases, the local maximum at the trough increases in magnitude and broadens in width such that the wave-form approaches that of a capillary-like wave with one-half the wavelength. That is, in figure 7, for example, as $\tilde{\sigma} \to 0{\cdot}85$, the computed profiles approach the shape of the capillary-like wave (of the same wave height) for which $\tilde{\sigma} = 4 \times (0{\cdot}85) = 3{\cdot}40$, since $\tilde{\sigma}$ is proportional to the

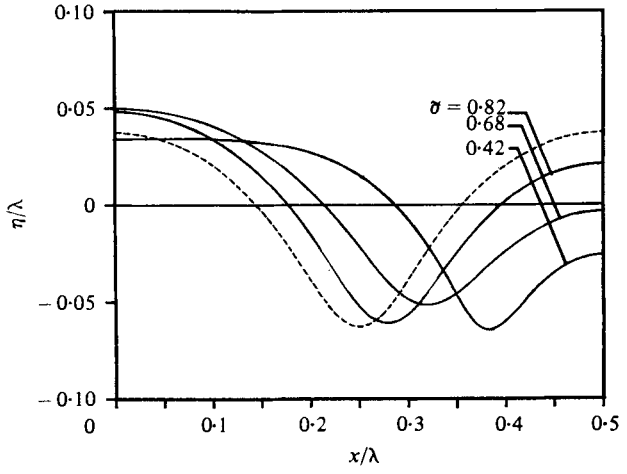

FIGURE 7. Surface profiles for the wave which is gravity-like at small amplitudes, calculated for $H/\lambda = 0{\cdot}10$ and various values of $\tilde{\sigma}$. The dashed line represents the profile for both $\tilde{\sigma} = 0{\cdot}85$ and $\tilde{\sigma} = 3{\cdot}4$.

square of the wavenumber. Because it is difficult to control to which solution of two very similar solutions the iteration procedure will converge, we cannot determine the merger point with great precision; therefore, $\tilde{\sigma} = 0{\cdot}85$ is only an estimate of the merger point. The second result is that the value of $\tilde{\sigma}$ for which this merger occurs increases with increasing H/λ; the merger occurs very close to $\tilde{\sigma} = 0{\cdot}545$ for $H/\lambda = 0{\cdot}01$ but for $H/\lambda = 0{\cdot}10$ the value of $\tilde{\sigma}$ is very close to 0·85. Therefore, for large H/λ, the range of $\tilde{\sigma}$ for which two distinct periodic waves exist is quite large.

The perturbation solution of Pierson & Fife suggests the behaviour described in the previous paragraph, although their solution is not quantitatively correct except for very small amplitudes and very close to $\tilde{\sigma} = 0{\cdot}50$.

The capillary-like wave was handled in very much the same way as the gravity-like wave. The calculation was started by using Harrison's approximate solution at $\tilde{\sigma} = 0{\cdot}58$ as the initial guess for the iteration procedure. Solutions were then found for progressively smaller values of $\tilde{\sigma}$ in a manner similar to that described for the gravity-like wave.

Figure 8 shows the free surface profiles computed at $\tilde{\sigma} = 0{\cdot}50$. These profiles have the general appearance of capillary waves, except that small depressions appear in the crests. Similar profiles were computed at $\tilde{\sigma} = 0{\cdot}42$ and 0·58. The depressions in the crests are small but increase in magnitude as $\tilde{\sigma}$ decreases. Also the maximum H/λ that we are able to compute decreases as $\tilde{\sigma}$ decreases.

Figure 9 is a plot of the computed speed versus wave height for the capillary-like wave compared with the phase speed computed from Pierson & Fife's approximate solution for the same three values of $\tilde{\sigma}$. The phase speed is seen to be a decreasing function of wave height in all three cases. Again, Pierson & Fife's solution appears to be accurate only for small amplitudes and close to $\tilde{\sigma} = 0{\cdot}50$.

The wave energies versus the wave height for $\tilde{\sigma} = 0{\cdot}50$ are plotted in figure 10; results calculated for $\tilde{\sigma} = 0{\cdot}42$ and 0·58 are very similar. The surface energy exceeds the gravitational potential energy at all wave heights.

The behaviour of these waves with $\tilde{\sigma}$, for two fixed wave height to wavelength

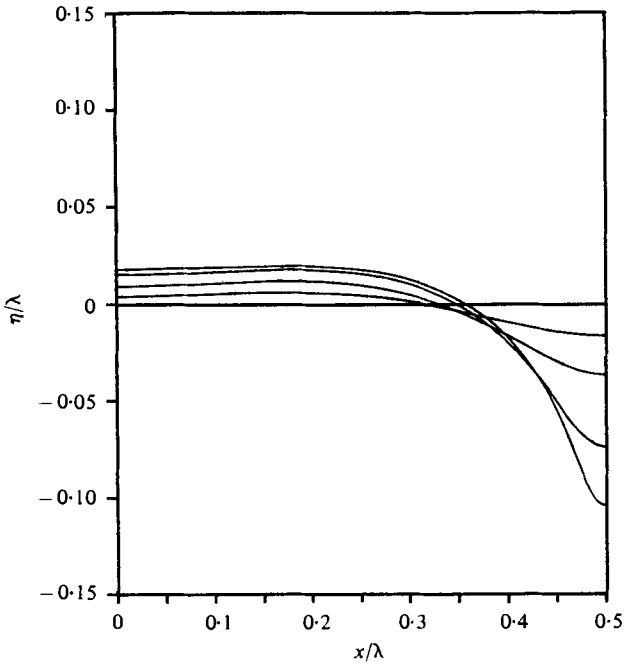

FIGURE 8. Surface profiles of the capillary-like wave, with $\tilde{\sigma} = 0{\cdot}50$, and $H/\lambda = 0{\cdot}02$, $0{\cdot}05$, $0{\cdot}09$, and $0{\cdot}12$. One half-wavelength is shown.

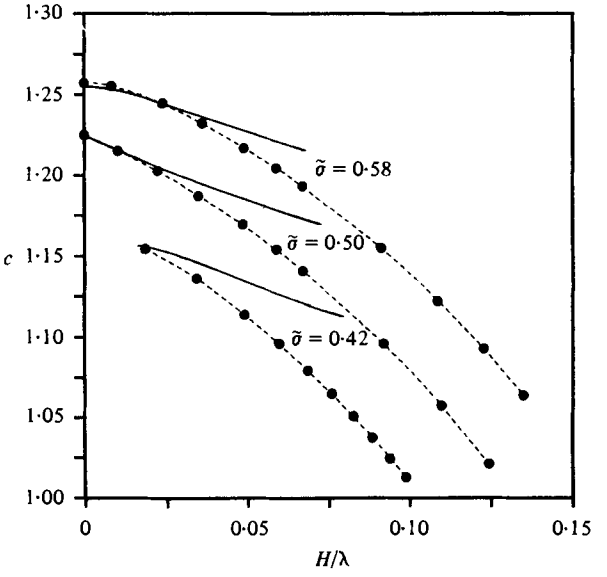

FIGURE 9. The phase speed as a function of the wave height for capillary-like waves. The present results (●) are compared with the approximate solutions (solid curves) of Pierson & Fife (1961). The dashed lines are spline fits to the present results.

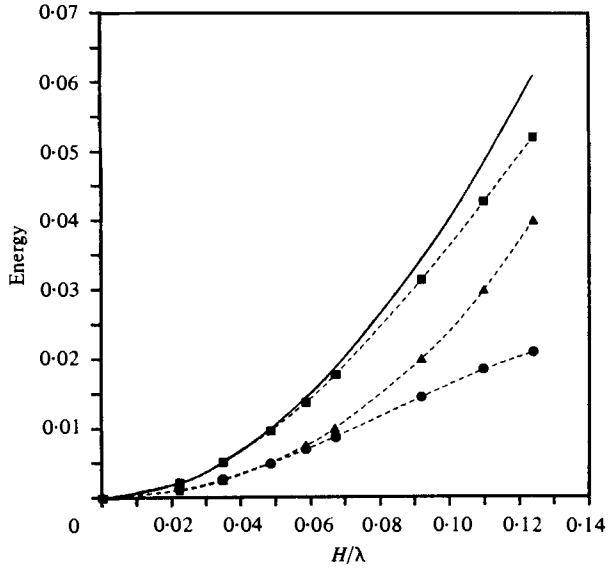

FIGURE 10. The calculated values of the kinetic energy (■), surface energy (▲) and gravitational potential energy (●) as functions of the wave height, calculated at $\tilde{\sigma} = 0{\cdot}50$ for a capillary-like wave. The dashed lines are spline fits to the present results, and the solid line is the sum of the surface and gravitational potential energies.

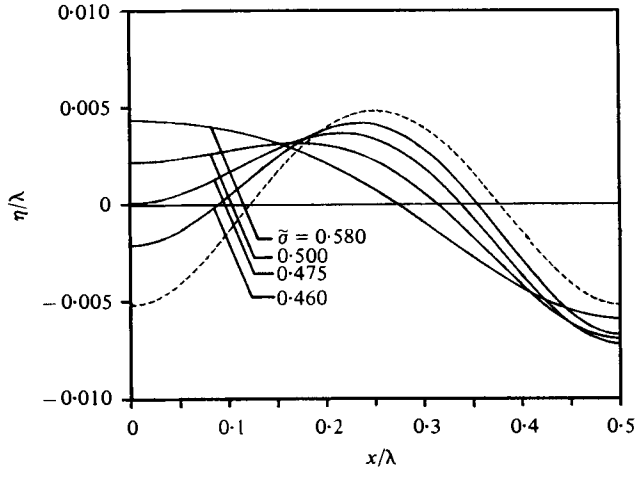

FIGURE 11. Surface profiles for a capillary-like wave, calculated for $H/\lambda = 0{\cdot}01$ and various values of $\tilde{\sigma}$. The dashed line represents the profile for both $\tilde{\sigma} = 0{\cdot}455$ and $\tilde{\sigma} = 1{\cdot}82$.

ratios, $H/\lambda = 0{\cdot}01$ and $0{\cdot}025$, is shown in figures 11 and 12. The results are analogous to the gravity-like case; the depression in the crest increases in magnitude and broadens in width as $\tilde{\sigma}$ decreases to the point where the waveform becomes indistinguishable from a capillary-like wave of twice its wavenumber. Note that the larger amplitude waves extend to smaller $\tilde{\sigma}$ values than the smaller amplitude waves. In particular, observe that the wave for which $H/\lambda = 0{\cdot}025$ exists as a distinct wave down to near the next singular point, $\tilde{\sigma} = \frac{1}{3}$.

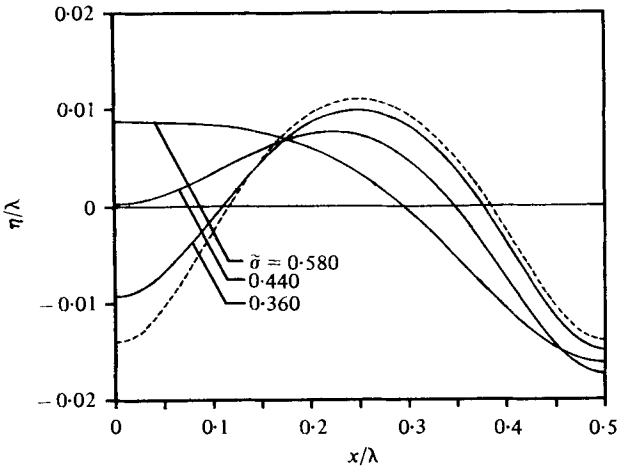

FIGURE 12. Surface profiles for a capillary-like wave, calculated for $H/\lambda = 0{\cdot}025$ and various values of $\tilde{\sigma}$. The dashed line represents the profile for both $\tilde{\sigma} = 0{\cdot}325$ and $\tilde{\sigma} = 1{\cdot}3$.

5. Conclusions

We have derived an integro-differential equation that describes gravity–capillary waves and that is convenient for numerical calculations.

For periodic gravity waves our numerical calculations verify the maxima in the phase speed and wave energy found by Longuet-Higgins (1975) and Cokelet (1977), who used Padé approximants.

The two gravity–capillary wave solutions found by Wilton (1915) and Pierson & Fife (1961) have been shown to have primarily capillary wave characteristics at large wave heights. Our calculations have also shown the approximate size of the wavenumber band for which two waves can exist; the size of the band increases with increasing wave height to wavelength ratio. The wave which is gravity-like at small amplitudes disappears at the large wavenumber end of the band, and the capillary-like wave disappears at the small wavenumber end. The mechanism by which the waves disappear is that the amplitudes of the fundamental and all odd multiples of the fundamental of the wave profile vanish, leaving a wave, in both cases, that is identical to a capillary-like wave having twice the wavenumber of the (disappearing) fundamental.

REFERENCES

BLOOR, M. I. G. 1978 Large amplitude surface waves. *J. Fluid Mech.* **84**, 167–179.

BYATT-SMITH, J. G. B. 1970 An exact integral equation for steady surface waves. *Proc. Roy. Soc.* A **315**, 405–418.

COKELET, E. D. 1977 Steep gravity waves in water of arbitrary uniform depth. *Phil. Trans. Roy. Soc.* A **286**, 183–230.

CRAPPER, G. D. 1957 An exact solution for progressive capillary waves of arbitrary amplitude. *J. Fluid Mech.* **2**, 532–540.

FOX, L. 1967 Romberg integration for a class of singular integrands. *Comp. J.* **10**, 87–93.

HARRISON, W. J. 1909 The influence of viscosity and capillarity on waves of finite amplitude. *Proc. Lond. Math. Soc.* **7**, 107–121.

KELVIN, LORD 1910 Ripples and waves. In *Mathematical and Physical Papers*, vol. 4, pp. 86–92. Cambridge University Press.

LEVI-CIVITA, T. 1925 Détermination rigoureuse des ondes permanentes d'ampleur finie. *Math. Ann.* **93**, 264–314.

LONGUET-HIGGINS, M. S. 1975 Integral properties of periodic gravity waves of finite amplitude. *Proc. Roy. Soc.* A **342**, 157–174.

MUSKHELISHVILI, N. I. 1953 *Singular Integral Equations*. Noordhoff.

NEKRASOV, A. I. 1921 On waves of permanent type I. *Izv. Ivanovo-Voznesensk, Politekhn. Inst.* **3**, 52–65.

PIERSON, W. J. & FIFE, P. 1961 Some nonlinear properties of long crested periodic waves with length near 2·44 centimeters. *J. Geophys. Res.* **66**, 163–179.

ROTTMAN, J. W. 1978 Numerical calculations of periodic gravity–capillary waves. Ph.D. dissertation, University of California, San Diego.

SASAKI, K. & MURAKAMI, T. 1973 Irrotational progressive, surface gravity waves near the limiting height. *J. Ocean. Soc. Japan* **29**, 94–105.

SCHWARTZ, L. W. 1974 Computer extension and analytic continuation of Stokes' expansion for gravity waves. *J. Fluid Mech.* **62**, 553–578.

STOKES, G. G. 1847 On the theory of oscillatory waves. *Trans. Camb. Phil. Soc.* **8**, 441–455.

STOKES, G. G. 1880*a* Supplement to a paper on the theory of oscillatory waves. In *Mathematical and Physical Papers*, vol. 1, pp. 314–326. Cambridge University Press.

STOKES, G. G. 1880*b* Considerations relative to the greatest height of oscillatory irrotational waves which can be propagated without change of form. In *Mathematical and Physical Papers*, vol. **1**, pp. 225–228. Cambridge University Press.

THOMAS, J. W. 1968 Irrotational gravity waves of finite height: a numerical study. *Mathematika* **15**, 139–148.

THOMAS, J. W. 1975 A numerical study of the relationship between the dimensionless parameters in the problem of periodic waves of permanent type in a liquid of finite depth. *Quart. Appl. Math.* **32**, 403–410.

WHITTAKER, E. T. & WATSON, G. N. 1927 *A Course of Modern Analysis*. Cambridge University Press.

WILTON, J. R. 1915 On ripples. *Phil. Mag.* **29**, 688–700.